Suspension Plasma Spraying of Nano-Ceramics Using an Axial Injection Torch

Oberste Berghaus, J.; Bouaricha, S.; Legoux, J.-G.; Moreau, C.; Chraska, T.

Publisher's version / Version de l'éditeur:

Proceedings. Thermal Spray 2005: Thermal Spray connects: Explore its surfacing potential!, pp. 1434-1440, 2005

NRC Publications Record / Notice d'Archives des publications de CNRC:
https://nrc-publications.canada.ca/eng/view/object/?id=6ca07e8e-f82d-4542-9a93-173c8ed76ab3
https://publications-cnrc.canada.ca/fra/voir/objet/?id=6ca07e8e-f82d-4542-9a93-173c8ed76ab3

IMI2004-107443-G CNRC 47592

Suspension plasma spraying of nano-ceramics using an axial injection torch

J. Oberste Berghaus, S. Bouaricha, J.-G.Legoux, C. Moreau, NRC Boucherville /CAN, T. Chráska, ASCR Praque /CZR.

Nanostructured coatings of Al_2O_3 and ZrO_2 (1.5% Y_2O_5) are produced by suspension plasma spraying, introducing the liquid feedstock internally into the central part of three converging plasma jets of a Mettech Axial III torch (Northwest Mettech Corp.). Spraying nanosized ceramic powders in a liquid carrier can yield thinner coatings with more refined microstructures than conventional plasma spraying. In-flight particle states are measured for a number of plasma conditions of varying torch current, gas flow rates and compositions (Ar, H_2, N_2), and related to the resulting microstructure and phase composition in the coatings, as determined by EDS, SEM and XRD. Results show that particle velocities up to 600 m/sec can be reached, yielding high impact velocities and cooling rates. Some comparison is made to previous work performed using external injection of a suspension droplet stream into a conventional dc plasma flame. At optimized conditions, dense γ-Al_2O_3 deposits with an average crystallite size below 30 nm are obtained at deposition efficiency above 80%, which was not previously attainable. Eutectic alumina-zirconia composite coatings with a finely layered lamellar structure are also realized. The laminates have potential advantages as thermal barrier coatings with beneficial properties arising from nano-composite components.

1. Introduction

Suspension plasma spraying using a liquid feedstock carrier, is an emerging technology, which permits the projection of much finer particles than conventional plasma spraying. Due to the finer lamellar structure, the formation of thinner (10-50µm) thermal spray coatings is possible [1-3]. Nano-structured coatings can be formed with this technique, since rapid solidification of the small impinging droplets restricts their gain growth. Certain mechanical and physical properties of materials exhibit remarkable improvements as their grain size is reduced to the nanometer range. Attractive features include decreased thermal diffusivity for thermal barrier coatings, increased ionic conductivity for solid oxide fuel cell components and improvements in hardness and ductility for protective coatings [4,5]. In dc suspension spraying, the liquid is commonly injected radially into the plasma flame external to the torch, either as a straight droplet jet [2][6] or atomized plume, for example [5]. Using an external droplet jet injector, previous work in our laboratory has shown that a high liquid jet velocity and precise injection location and angle with respect to the central part of the plasma flame is critical to ensure effective heat transfer, which leads to adequate coating formation. A small injection nozzle opening was suitable to fulfill the velocity requirement, without exceeding the finite loading capacity of the plasma [7]. However, slight injection instabilities, for instance caused by nozzle obstructions, lead to severe loss in process efficiency. Diagnostics on the plasma spray plume suggested that the particle created in flight are often so small (< 2 µm) that they effectively follow the plasma gas velocity in the free stream, as well as in the viscous boundary layer in front of the substrate. This can lead to reduced particle impact velocities for lighter materials, such as aluminia, preventing dense and nano-structured coating formation [7].

Building on this research, the need for improved process robustness, increased loading capacities and wider operating ranges, in particular, higher particle velocities for some materials, was identified. In this study, the suspension feedstock is axially injected into a Mettech Axial III torch (Northwest Mettech Corp.), thereby fully entraining the droplets by the encircling three plasma streams. Zirconia and alumina coatings are produced. The aim is to reduce the process sensitivity to the injection conditions, maximize the heat and momentum transfer from the plasma, and extend the processing range. In-flight particle velocities and temperatures are measured for different operating conditions of the torch and related to the resulting deposition efficiencies and microstructure of the coatings. Finally, micro-composite coatings from eutectic Al_2O_3-ZrO_2 feedstock are presented, and the prospect of nanocomposite formation is assessed.

2. Experimental

The suspension spraying system uses a Mettech Axial III torch, equipped with an internal injection /atomization module. A photograph of the suspension plume is shown in **Fig.1**. The suspension is delivered by a positive-displacement dosing pump from an agitated reservoir, and measured by a precision flowmeter. By ensuring continuous flow and agitation in all wetted conduits during spraying and idle operation, sediment formation, which can cause malfunction of the solenoid valves and injector, is avoided. Startup, shutdown, as well as rinsing and final ethanol washing sequences of the conduits and torch interior are fully automated and PC controlled.

The suspensions of 10 wt% solids in ethanol are prepared for α-Al_2O_3 (29-68nm), as well as a 50/50 mixture of undoped (29-68 nm) to 3wt% yttria doped ZrO_2 (80nm) (Nanostructured & Amorphous Materials, Los Alamos, USA), yielding a zirconia powder with a 1.5wt% average yttria content. A suspension of 57 wt% Al_2O_3 and 43 wt% ZrO_2 (1.5%Y) is also prepared by mixing the two feedstocks. At this ratio, a eutectic Al_2O_3-ZrO_2 alloy exists. The powders are dispersed in an ultrasonic bath. No additional dispersant is added.

Coatings are produced on 100-grid sandblasted mild-steel substrates.

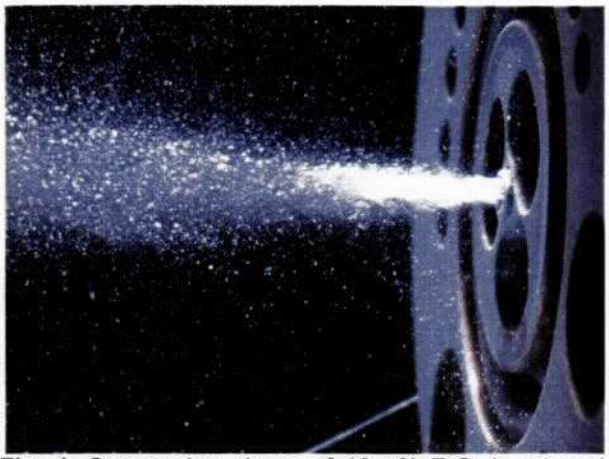

Fig. 1. Suspension plume of 10wt% ZrO_2 in ethanol exiting the torch divergence at 0.04 slpm.

Microstructures are observed by SEM (Jeol JSM-610) and FE-SEM (Hitachi S4700). The samples are prepared by standard metallographic methods. Porosity is assessed from cross-section SEM (500X), using image analysis. The intensity range and thresholds are standardized on reference materials, and ten measurements are averaged per sample. This method is well suited to rank porosities of conventional thermal spray coatings. It is limited, however, to capture some of the finer porosity and nano-pores encountered in this study. Thermal diffusivity α is evaluated for selected samples using a laser flash method. The thermal conductivity k of these coatings is determined using the relationship $k = \alpha C_p \rho$. Specific-heat (C_p) measurements for Al_2O_3-ZrO_2 coatings are made using a standard differential scanning calorimeter (DSC-2, Perkin-Elmer), with sapphire as a reference material. Phase analysis is carried out by XRD using a Brucker D8-Discovery diffractometer with Cu-K_α radiation at an acquisition of 0.01°/sec. The crystallite size is evaluated from the Sherrer equation and, where applicable, Williamson-Hall type plots. Further details are described elsewhere [7].

In-flight particle states are measured with a commercial diagnostic system (AccuraSpray® G2 Tecknar, Canada), acquiring the thermal radiation of the particles through two closely spaced optical fibers. The temperature measurement is based on two-colour pyrometry, and the velocity is determined by a time-of-flight technique, making use of a cross-correlation calculation. The measurement volume is centered in the spray plume at 50 mm from the torch exit nozzle, i.e. at the location of the substrate during deposition. The measurement is sufficiently far from the plasma flame, such that the gas radiation does not influence the pyrometric reading. Since the small size of the ceramic particles in-flight prevents individual particle detection, an ensemble particle diagnostic system, which senses the fluctuations of the total emitted radiation in the field of view, is deemed necessary [7].

3. Results and Discussion

3.1 Spray Conditions

The plasma torch is operated at four different conditions of varying gas flow rate and composition, which are expected to yield distinct differences in the particle states, as summarized in **Table 1**. Minimizing electrode erosion, the current is adjusted to limit the torch power to approximately 90 kW.

Table 1: Plasma operating conditions

Cond.	Torch current x3	Gas Flow (slpm)	Ar %	N_2 %	H_2 %	Power (kW)
1	160 A	120	10	80	10	73
2	190 A	140	20	70	10	87.5
3	180 A	180	45	45	10	86.3
4	200 A	245	75	10	15	83.2

3.2 In-flight Particle States

The measured particle states are summarized in **Table 2**. With an increase in gas flow rate and argon concentration, particle velocities up to 600 m/sec can be generated. Such high velocities are rarely attained in atmospheric plasma spraying. Our previous work has shown that for small particles entrained in an impinging plasma flow, a faster jet can dramatically increase the particle impact velocity during the coating formation, possibly leading to an improved flattening ratio of the spats. The very high velocity of cond. 4 comes, however, at the expense of a reduced particle temperature, possibly due to a lesser heat transfer at lower nitrogen plasma composition and a shorter residence time of the particles in the heating plasma flame.

Table 2. Particle states for the selected spray conditions at a flowrate of 1.8 kg/hr.

	10% Al_2O_3		10% ZrO_2		10% Al_2O_3-ZrO_2 solids in EtOH	
Cond.	V_{part} (m/sec)	T_{part} (°C)	V_{part} (m/sec)	T_{part} (°C)	V_{part} (m/sec)	T_{part} (°C)
1	263	2610	273	2600	-	-
2	-	-	-	-	390	2880
3	500	2700	526	2851	518	2716
4	574	2520	600	2512	600	2557

Reducing the suspension flowrate can partially compensate the loss in particle temperature. By varying the flowrate of a 10% ZrO_2 suspension between 19.3 ml/min and 48.2 ml/min, distinct temperature variations are introduced at nearly constant particle velocity, as shown in **Fig. 2**. The coatings shown in the following sections are produced at a constant mass flowrate of ~1.8 kg/hr (34.7 ml/min for 10% ZrO_2).

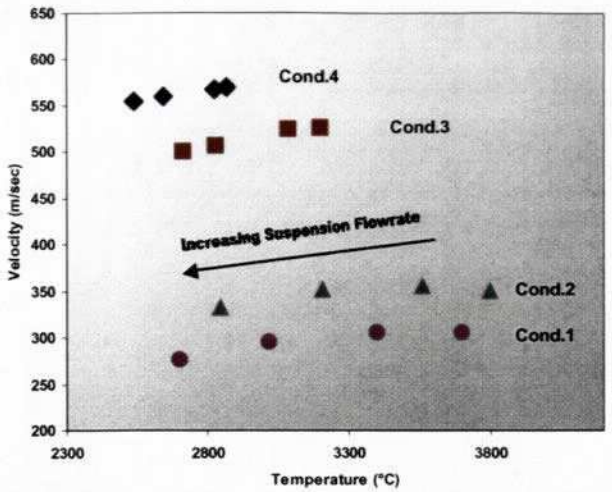

Fig. 2. Particle states of 10% ZrO_2 in ethanol at 63.5 mm from torch nozzle; Flowrates: 19.3 to 48.2 ml/min.

3.3 Alumina

Typical SEM micrographs for the alumina coatings from spray conditions 1,3 and 4 are shown in **Fig. 3**. The substrate temperature is maintained at approx. 400°C. Deposition efficiency and porosity values are summarized in **Table 3**. A fine-structured open porosity is created at low particle velocity (cond.1), resembling the deposits previously obtained with an external injection system [7]. A significant densification and higher deposition efficiencies are attained with increasing particle velocity (cond. 3). The higher resulting impact velocities likely impart an improved spreading of the individual spats [2]. Furthermore, fewer of the particles in the smallest size ranges are entrained in the viscous boundary layer flow and thereby deflected from the substrate. Further increase in particle velocity (cond. 4) leads to deposition efficiencies of 84%. However, the lower particle temperature, associated with this operating condition, reintroduces some porosity by allowing in-flight solidification of very fine particles, which were identified in the coating at high magnification. Considering the low thermal inertia of micron-sized alumina particles [1], particle temperatures far above the melting point are beneficial in preventing such in-flight solidification.

Table 3. Summary of Al_2O_3 deposits.

Cond.	D.E. (%)	Porosity (%)	Approx. γ-Al_2O_3 content	Grain size (nm)	
				α-Al_2O_3 W.H.	γ-Al_2O_3 Sherrer
Feed			23 %	59	-
1	48%	44 ± 1.5	68 %	40	31 ± 5
3	69%	11 ± 5	88 %	-	25 ± 10
4	84%	21 ± 2	80 %	29	27 ± 6

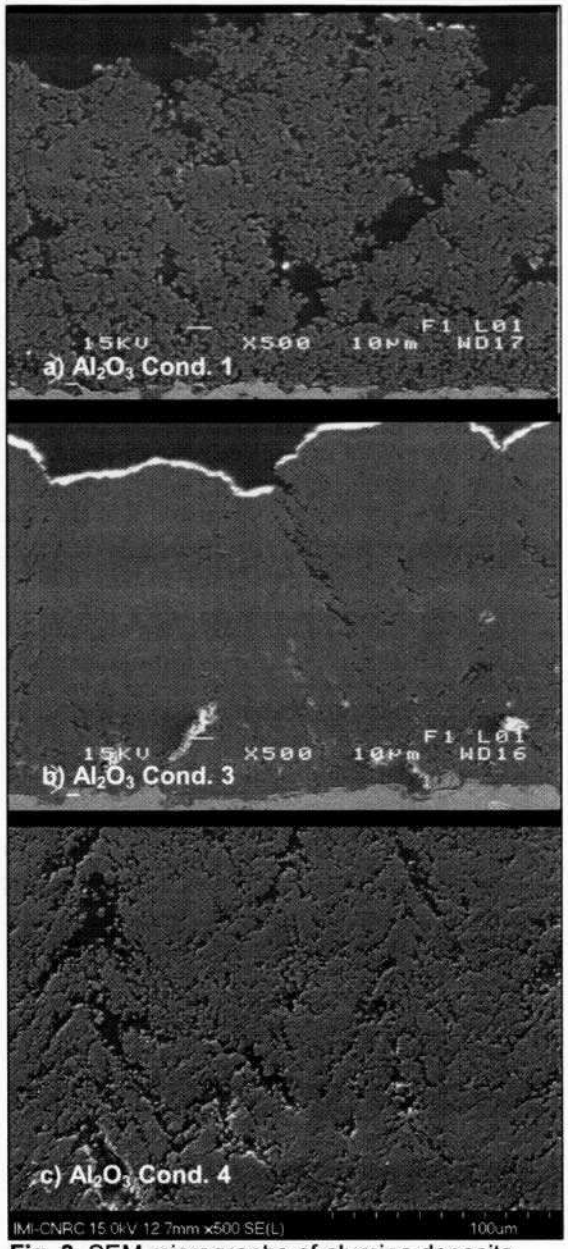

Fig. 3. SEM micrographs of alumina deposits.

The XRD spectra in **Fig. 4** are summarized in **Table 3**. Comparing cond. 4 to cond. 1 reveals smaller crystal grain sizes and a higher retention of the metastable γ-phase with higher particle velocities. Further grain refinement is attained with an additional increase in particle temperatures, as seen for cond. 3. In the plasma spray process, the grain size and phase is traditionally linked to the cooling rate at rapid solidification, see [7] and references therein. Higher flattening ratios and thinner splats, induced by both higher impact velocities and lower viscosities of the impacting droplets, as well as an increased thermal conduction through the denser coatings are contributing to the elevated quench rates. An additional factor is the virtual absence of in-flight solidified particles at cond.3.

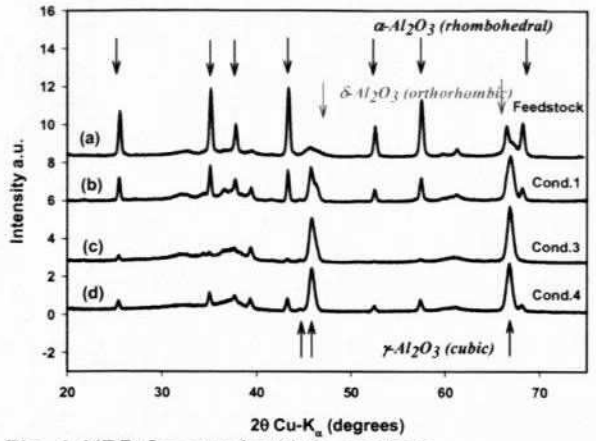

Fig. 4. XRD Spectra for Al_2O_3 coatings.

3.4 Zirconia

Highly dense and crack free coatings of ZrO_2-1.5 wt% Y_2O_3 are produced at all plasma conditions investigated, as shown in representative micrographs in **Fig. 5**. The coating characteristics are summarized in **Table 4**. Contrary to our experience with the external injection system, initial spray tests with pure zirconia feedstock resulted in coating detachment and spalling. The following measures were implemented to reduce the compressive stress in the films: The material was stabilized with yttria to reduce the volume expansion of the tetragonal to monoclinic phase transformation. The substrate temperature during spraying was reduced to 180°C-200°C in order to minimize the cooling stresses, which arise from the CTE mismatch, and the coating thickness was reduced.

Doubling the particle velocity from 270 m/sec (cond.1) to 530 m/sec (cond. 3), results in a densification of the coating, an improvement in deposition efficiency and complete disappearance of any visible lamellar structure. Besides an enhanced spreading of the hotter particle splats at this condition, the higher capture of small-sized particles may explain the D.E. improvement [7]. Without substantial raise in micron-sized porosity, further increase in velocity (cond.4) introduces embedded zones, which resemble the morphology of the original feedstock powder, and are likely semi-molten particles [6]. These can arise by virtue of the high melting point of zirconia (~2700°C), considering the lower average particle temperature and short residence time at cond.4. See **Fig.5 c)**.

Table 4. Summary of ZrO_2- 1.5wt%Y_2O_3 deposits.

Cond.	D.E. (%)	Porosity (%)	t-ZrO_2 content	Grain size (nm)	
				m-ZrO_2 Sherrer (W.H.)	t-ZrO_2 Sherrer (W.H.)
Feed			34 %	26 ± 1 (25)	26 ± 10 (29)
1	55%	1 ± 0.3	83 %	30 ± 2 (28)	31 ± 6 (36)
3	64%	0.1 ± 0.02	77 %	31 ± 5 (23)	30 ± 5 (36)
4	54%	0.2 ± 0.04	78 %	32 ± 1 (28)	31 ± 4 (42)

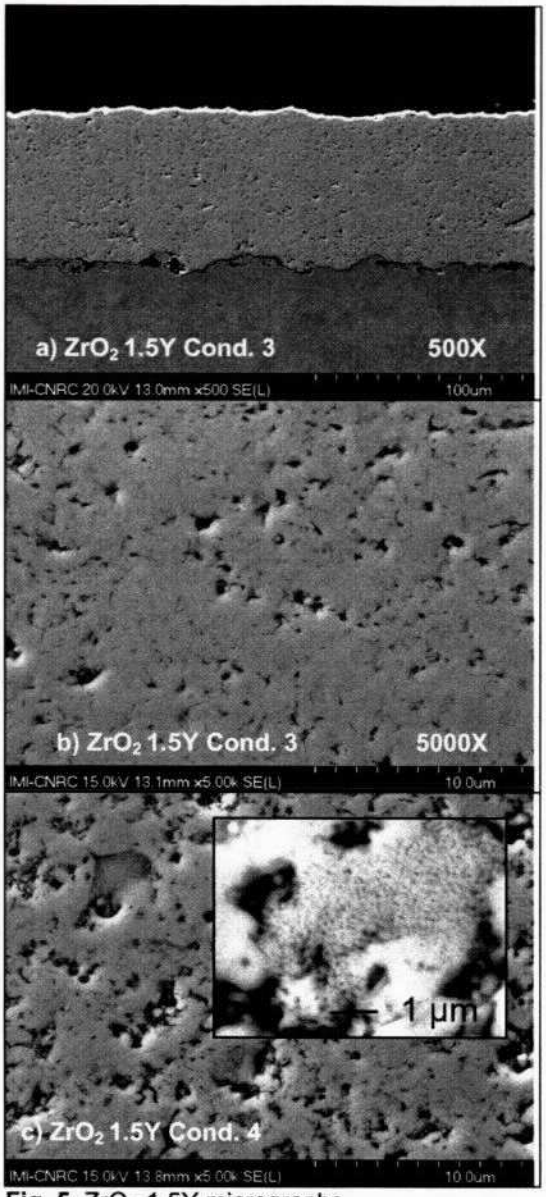

Fig. 5. ZrO_2-1.5Y micrographs

For zirconia, we had previously observed that high in-flight particle temperatures lead to smaller crystal grain sizes, which was rationalized by the creation of thinner splats from very liquid droplets [7]. Based on that finding, a grain size larger than the original feedstock, as estimated in **Table 4.**, is a consequence of low particle temperatures, barely at the melting point of zirconia, at the chosen flowrate. Ultimately, however, the zirconia coatings produced in this study resemble the deposits previously obtained with the external injection system.

3.5 Eutectic Al_2O_2-ZrO_2

Micro-composite coatings of alumina and zirconia are shown in **Fig. 6**. A substrate surface temperature of approximately 300°C is maintained for all spray conditions. A feedstock composition of 57% Al_2O_3 and 43 % ZrO_2 is chosen, since the binary phase diagram features an eutectic point with a lowering of the liquid

curve to 1900°C [8]. Besides creating thin, alternating layers, the underlying motivation is to induce, at least partially, an amorphous or nanocomposite structure by melt-quenching the ceramic solution in the spray process, preventing eutectic phase formation [8]. Alumina nanocomposites can suppresses t-ZrO_2 to m-ZrO_2 transformation by increasing the critical nucleus size in a constraining matrix [9]. Improvement in mechanical properties compared to both alumina and zirconia ,i.e. higher fracture toughness and slow crack growth, are reported in the literature [10]. Furthermore, a low thermal conductivity in multilayer Al_2O_3-ZrO_2 coatings is generally measured [11], which is not solely attributed to the interface resistance [12], but to the existence of crystalline nano-grains [13]. For the application in thermal barrier coatings, a continuous alumina stratum could further serve as an oxygen diffusion barrier to reduce the thermally grown oxide layer at the bond coat interface [12].

Table 5 illustrates that high deposition efficiencies are attained, higher than for zirconia alone. Furthermore, the porosities are substantially lower than for pure alumina. Both effects are likely due to some interaction of the two materials. The particle momentum is increased by the zirconia content, leading to higher impact velocities; the melting point is to some extent lowered by the eutectic reaction; and splashing, which can create overspray losses in zirconia splats, [7] may be reduced by the alumina.

The micrographs feature distinct compositional layers, indicating limited dissolution of the primary alumina and zirconia powder during the brief thermal transient in the liquid state. In an individual particle, segregation is likely initiated by early on melting of the Al_2O_3 with respect to the still unmolten ZrO_2 [13], invoking solid-liquid phase separation. The large difference in melting points fosters the incongruent melting. Some imperfect powder mixing, as verified by EDS mapping of the dried suspension, also favors separation at the outset. As a consequence of the high particle velocities, the short residence time in the plasma allows only modest subsequent liquid mixing and homogenization in a completely molten particle [14][8]. Regions of intimate mixing, reflected by the light gray structures in the micrographs, are found predominantly in the vicinity of the white zirconia splats, as halos. This supports the idea that the composition in individual particles is segregated, but some liquid phase diffusion occurs at the zirconia-alumina interfaces.

In addition to a higher porosity at Cond. 4, examination of the micrographs in **Fig. 6** reveals a refinement in the layer structures with increasing particle velocity (Cond.2 to 4). Similar to pure alumina, more of the smaller-sized particles/splats, homogenized or still segregated, are likely incorporated into the coating at the higher velocity.

The zirconia splats show transverse cracks (visible only at higher magnification), which are caused by the lower thermal expansion coefficient of Al_2O_3, placing the ZrO_2 layers in residual biaxial tension [15]. At very low particle velocity and high temperature (cond. 1, no photo), the deposit showed a curling behavior, detaching from the substrate altogether. On the basis of the coarsening lamellar structure, we speculate that the stresses in thick and well-ordered layers are the reason for the failure.

Table 5. Summary of Al_2O_3-ZrO_2-1.5wt%Ydeposits

Cond.	D.E. (%)	Porosity (%)	t -ZrO_2 content (% in ZrO_2)	m-ZrO_2 Sherrer	t-ZrO_2 Sherrer	γ-Al_2O_3 Sherrer
2	66	0.4 ± 0.1	83	18 ± 7	23 ± 2	35 ± 2
3	75	0.7 ± 0.1	87	18 ± 8	21 ± 2	34 ± 3
4	69	1.1 ± 0.2	81	23 ± 2	21 ± 3	28 ± 3

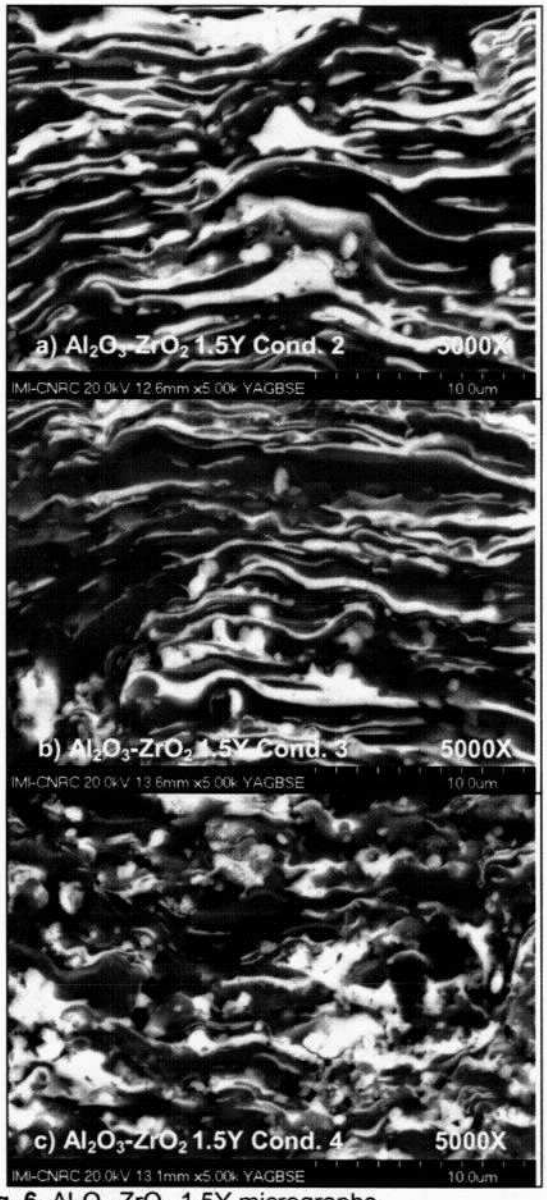

Fig. 6. Al_2O_3-ZrO_2-1.5Y micrographs.

The XRD spectrum in **Fig. 6** does not identify a distinct amorphous phase. However, EDX scans through the light gray regions of the micrograph suggest some intimate compositional mixing. Comparison of the XRD spectrum with zirconia, deposited under identical torch operating conditions,

shows a higher content of the metastable tetragonal phase and a refinement in grain size, as shown in **Table 5**. These are indications that some nano-composite constituents are likely present in the coatings.

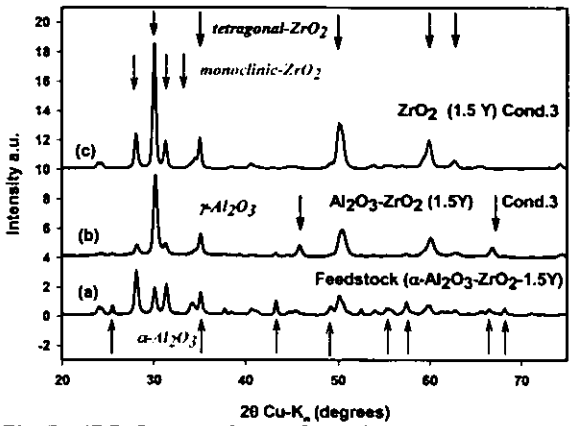

Fig.7. XRD Spectra for Al_2O_3-ZrO_2 and ZrO_2-1.5Y.

To assess the potential of these coatings for thermal barrier applications, the thermal conductivity of the composite coating from cond. 3 was measured as 1.7 ± 0.01 W/mK, which compares favorably with an equally thick and dense ZrO_2 coating, for which a conductivity 2.7 ± 0.02 W/mK was measured.

4. Conclusions

- An axial feed suspension plasma spraying system is implemented. An improved robustness over a radial injection system makes process automation viable.
- The processing range in terms of particle states is extended to velocities up to 600 m/sec. Reduction in particle temperatures, associated with the high velocity conditions, can be compensated by adjusting the suspension loading of the plasma.
- For alumina, higher particle velocities translate into high deposition efficiencies up to 84%, relatively low porosities (11%), high retention of the metastable phase and grain size refinement to 30 nm or less, which was not previously attained in our laboratory. Further improvement necessitates elevated particle temperatures to counter in-flight solidification of the smaller particles.
- Zirconia is less sensitive to the particle velocity conditions, and dense coatings are produced in all cases. However, low dwell times can lead to incomplete particle melting.
- Microcomposite Al_2O_3-ZrO_2 coatings, with promising properties for thermal barrier applications, are realized. At some operating conditions, higher deposition efficiencies, grain refinement and lower porosities are attained than for the constituents sprayed individually. The brief thermal transient in the liquid phase limits homogenization, resulting in a compositionally layered structure. High particle velocities increase small particle capture, ensuing layer refinement. An ongoing optimization focuses on the characteristics and properties of these coatings.

Acknowledgement

Technical support from B. Harvey for process automation, S. Belanger for thermal spraying, M. Lamontagne for particle diagnostics, J.-F Alarie for sample preparation and M. Thibodeau for XRD and SEM analysis is gratefully acknowledged.

References

[1] Fauchais, P.: Understanding plasma spraying, J.Phys.D: Appl. Phys. 37 (2004) R86-R108.

[2] Delbos C., Fazzilleau, J., Rat, V. Couder J.F., Fauchais, P.: Finely structured ceramic coatings elaborated by liquid suspension injection in a DC plasma jet, Proc. of ISTC 2004 (pdf.file), Osaka, Japan; DVS, Germany.

[3] Karthikeyan,J., Berndt, C.C., Reddy, S, Wang J-Y., King A.H. Herman, H.: Nanomaterial deposits formed by DC plasma spraying of liquid feedstocks, J.Am.Ceram.Soc. 81 (1998), Issue 1, pp.121/28.

[4] Bouaricha S., J. Oberste Berghaus, J.-G.Legoux, D. Ghosh, S. Moreau: Production of samarium doped ceria plasma sprayed nano-coatings using an internal injection of a suspension containing nanoparticles. Proc. of ITSC 2005, Basel, Switzerland. DVS, Düsseldorf, Germany.

[5] Jordan E.H., L. Xie, X. Ma, M. Gell, N.P. Padture, B. Cetegen, A. Ozturk, J. Rogh, T.D.Xiao, T.E.C. Bryant: Superior thermal barrier coatings using solution precursor plasma spray; Journal of Thermal Spray Technology, Vol. 13 (2004) (1) p. 57-65

[6] Siegert R., J.-E.Döring , J.-L. Marqueés, R. Vaßen, D. Sebold, D. Stöver: Denser ceramic coatings obtained by the optimization of the suspension plasma spraying technique, Proc. of ISTC 2004 (pdf.file), Osaka, Japan; DVS, Düsseldorf, Germany.

[7] Oberste Berghaus J., S. Bouaricha, J.-G. Legoux , C. Moreau: Injection conditions and in-flight particle states in suspension plasma spraying of alumina and zirconia nano-ceramics. Proc. of ITSC 2005, Basel, Switzerland. DVS, Düsseldorf, Germany.

[8] Zhou X., V.Shukla, W.R. Cannon, B.H.Kear: Metastable phase formation in plasma-sprayed ZrO_2 (Y_2O_3)-Al_2O_3. J.Am.Ceram.Soc. 86 (2003), Issue 8, pp.1415/20.

[9] Andritschky M., I. Cunha, P. Alpuim: Thermal stability of zirconia/alumia thin coatings produced by magnetron sputtering. Surface and Coatings Technologies 94-95 (1997) Issue 1-3 pp.144/48.

[10] Deville S., J. Chevalier , G. Fantozzi, J.F. Bartolomé, J. Rquena, J.S. Moya, R. Torrecillas, L. A. Díaz: Low-temperature ageing of zirconia-toughened alumia ceramics and its implication in biomedical implants. J. Eu. Ceram. Soc. 23 (2003) pp. 2975/82.

[11] Ravichadran K.S., K. An: Thermal conductivity of plasma-sprayed monolithic and multilayer coatings of alumina and yttria-stabilized zirconia. J.Am. Ceram. Soc. 82 (1999), Issue 3, pp. 673/82.

[12] Sharafat S., A. Kobayashi, Y. Chen, N.M. Ghoniem: Plasma spraying of microcomposite thermal barrier coatings. Vacuum 65 (2002) pp. 415/25.

[13] Sodeoka S., M. Suzuki, T. Inoue: Thermal and mechanical properties of alumina-zirconia nano-composite coating. Proc. of ISTC 2004 (pdf.file), Osaka, Japan; DVS, Düsseldorf, Germany.

[14] Manger J., W.R. Cannon, B.H. Kear: Plasma reaction synthesis of agglomerated oxide powders by axial injection torch. Proc. of ISTC 2004 (pdf.file), Osaka, Japan; DVS, Düsseldorf, Germany.

[15] Cai P.Z., D.J. Green, G.L. Messing: Constrained densification of alumina/zirconia hybrid laminates. J. Am. Ceram. Soc. 80 (1997), Issue 8, pp.1929/39.